Open-Structure Resonant Technique for Measuring the Dielectric Properties of Materials

William R. Humbert, *Member, IEEE*, and Waymond R. Scott, Jr., *Member, IEEE*

***Abstract*—A newly developed resonant measurement technique is extended to include rotationally symmetric materials in general. The technique involves a full wave analysis of the fixture containing the material under test. Therefore, the measurement technique is not restricted by the dimensions of the material or its electrical properties. This work describes the measurement technique and provides a characterization of the TE_{011} resonant mode. Also, a method to account for conduction loss due to the surface resistance of the metal walls of the fixture is presented. Experimental results are compared to previously reported values and are in excellent agreement.**

***Index Terms*— Dielectric measurements, resonator, finite-element method, loss tangent, permittivity.**

I. Introduction

THE increased use of low-loss dielectric materials in electronic devices emphasizes the need to accurately measure their electrical properties. By doing so, models used to predict the performance of devices utilizing these materials are more accurate and reliable. The authors previously introduced a new resonant technique for measuring dielectric rods [1], and later extended the work to include dielectric sheets [2]. After further investigation, the technique has been extended to include rotationally symmetric materials in general. The presented work outlines the principles surrounding the measurement technique, characterizes the TE_{011} resonant mode for the fixture, and includes a method to characterize the surface resistance of the metal walls of the fixture.

The fixture used in this measurement technique is rotationally symmetric and is shown in Fig. 1 in the $\rho - z$ plane. It consists of two rotationally symmetric metallic plates placed opposite each other, where each plate has a central opening leading to an extended tubular section. In this configuration, the fixture has circular and radial waveguide regions with heights, h, and diameters, D, denoted by subscripts c and r, respectively. At the junction of these waveguide regions is the core of the resonator. The material, or a portion of the material, is position within the core of the resonator. Then, with properly chosen dimensions, h_r and D_c, the excited resonant mode will be confined in the region near the core of the resonator and produce exponentially decaying fields in the circular and radial waveguide regions. This behavior is illustrated in Fig. 2. As a result of the exponential decay of the field, the dimensions h_c and D_r can be chosen to be finite quantities.

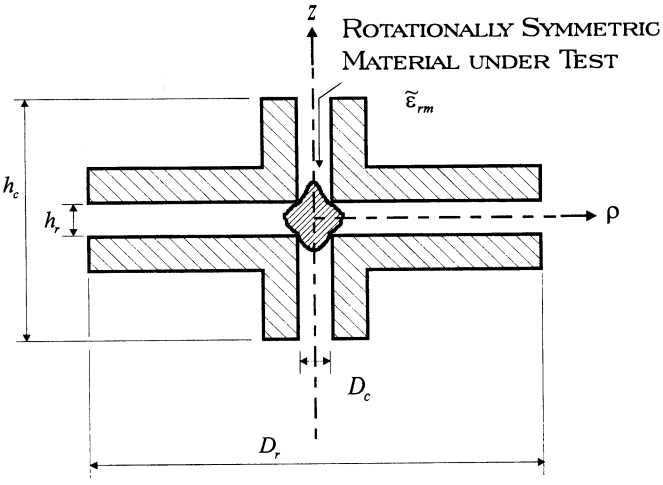

Fig. 1. Fixture used to measure the dielectric properties of rotationally symmetric materials.

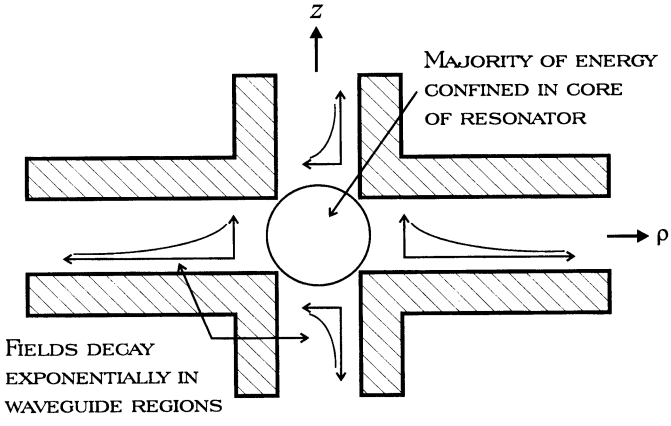

Fig. 2. Illustration of resonant behavior in the various regions of the fixture.

It should be noted that G. Kent has used a similar device to determine the dielectric properties of substrates, however the circular waveguide regions are terminated by a conductor [3]. In his analysis, the energy coupled to the radial waveguide region is neglected and the fixture is modeled as a circular cavity. Later, a perturbational technique is applied to estimate the error associated with neglecting the energy coupled to the

Manuscript received November 10, 1997; revised November 30, 1998.

W. R. Humbert is with the Sensors Directorate, Air Force Research Laboratory, Hanscom AFB, MA 01731 USA.

W. R. Scott, Jr. is with the School of Electrical and Computer Engineering, Georgia Institute of Technology, Atlanta GA 30332 USA.

Publisher Item Identifier S 0018-9456(98)09808-8.

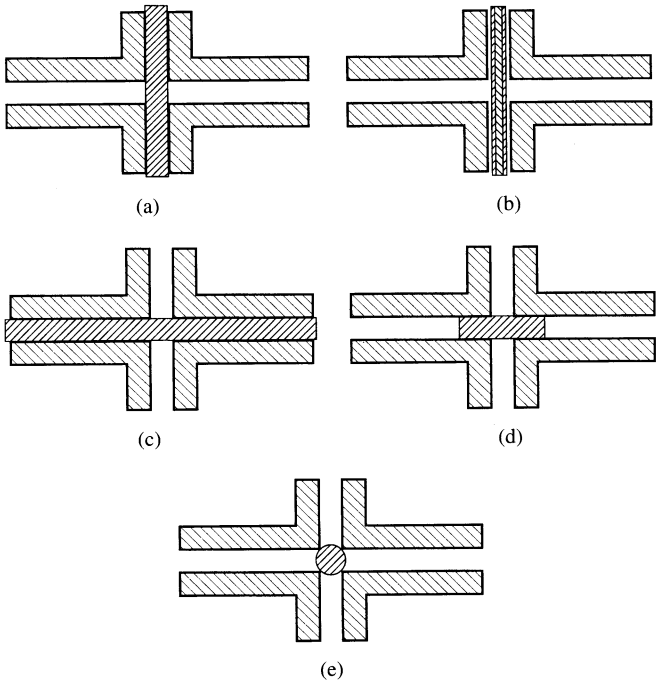

Fig. 3. Configurations used to measure the dielectric properties of dielectric: (a) rods, (b) tubes (also liquid filled), (c) sheets, (d) disks, and (e) spheres.

radial waveguide. This can place restrictions on the geometry and/or the dielectric constant of the substrate. The presented measurement technique uses a full-wave analysis of the fixture and, thus, is not constrained by the geometry or dielectric constant of the material under test.

In this work, experimental results are presented for dielectric rods, tubes, sheets, disks, and spheres. The configurations used for each of the material types is shown in Fig. 3. The materials investigated range in permittivity from 2 to 24, and in loss tangent from 10^{-5} to 10^{-3}.

II. Analysis

The dielectric material under test is assumed to be linear, isotropic, homogeneous, and nonmagnetic ($\mu = \mu_0$). Thus, the material can be characterized by the complex effective relative permittivity $\tilde{\epsilon}_{rm} = \epsilon_{rm} - j\sigma_m/\omega\epsilon_0$, with the relative permittivity $\epsilon_{rm} = \epsilon'_{rm} - j\epsilon''_{rm}$, conductivity σ_m, and the permittivity of free space ϵ_0. The effective relative permittivity can also be expressed as $\tilde{\epsilon}_{rm} = \epsilon'_{rm}(1 - j\tan\delta_m)$, with the loss tangent $\tan\delta_m = \epsilon''_{rm}/\epsilon'_{rm} + \sigma_m/\omega\epsilon'_{rm}\epsilon_0$.

Because of the complex geometry of the fixture, the finite-element method (FEM) is used to model the fixture containing the material under test. The FEM makes use of vector basis functions as described in [4] and is outlined in detail in [5]. Taking advantage of rotational symmetry allows the finite-element problem to be reduced to a two-dimensional formulation involving the known azimuthal variation. The finite-element formulation results in a generalized eigenvalue problem where the eigenvalue is associated with the resonant frequency and the eigenvector is the field distribution of the resonant mode.

Because this research is primarily concerned with low loss materials (i.e., $\tan\ \delta_m \ll 1$), a perturbational technique is used to account for the loss. It can be assumed that the electromagnetic field will not change significantly because of the loss. The quality factor can then be determined using the electromagnetic field calculated by the FEM. Since the time-average energy stored in the electric field is equal to that of the magnetic field at resonance, the quality factor can be expressed as

$$Q = \frac{2\omega_0 W_e}{P_l} \tag{1}$$

where ω_0 is the angular resonant frequency, W_e is the time-average energy stored in the electric field, and P_l is the total time-average power loss in the *system*. In general the system includes the resonator and some external circuitry used to perform the measurements. For this work, the external circuitry consists of a pair of measurement probes connected to a network analyzer. The positioning of the probes, while inside the measurement fixture, is easily controlled. The ability to directly withdraw or rotate the probes allows control over the amount of coupling. If the amount of coupling can be minimized such that no changes in the resonant frequency or quality factor occurs, then the effect of the coupling loops is negligible [6], [7]. During experimental measurements, the probes are withdrawn from the core of the resonator until there is no detectable change in the resonant frequency and quality factor. Therefore, the effect of the probes is negligible and P_l is the time-average power loss in the resonator.

For the described resonator, there are basically three mechanisms which contribute to the total time-average power loss. These include: power dissipated in the dielectric, power dissipated on the conducting walls of the fixture, and power radiated out of the ends of the waveguide regions. Because of the decaying behavior of the field in the waveguide regions, the power radiated out is negligible for sufficiently long waveguides regions. Therefore, the total time-average power loss is the sum of the dielectric loss and conduction loss written as

$$P_l = P_d + P_c \tag{2}$$

where P_d is the time-average power dissipated in the dielectric and P_c is the time-average power loss due to the surface currents on the walls of the fixture. Assuming P_d and P_c are independent, the quality factor in (1) can be expressed in terms of partial quality factors as

$$\frac{1}{Q} = \frac{1}{Q_d} + \frac{1}{Q_c} \tag{3}$$

where the subscripts d and c denote dielectric and conductor, respectively.

III. The TE_{011} Mode

The TE_{011} mode is used to reduce measurement errors associated with air gaps at dielectric-conductor interfaces. Having only H_z, H_ρ, and E_ϕ field components, this mode has no electric field normal to the air gaps. Therefore, measurements are not strongly affected by the air gaps.

There are no closed-form expressions for this mode near the core of the resonator. However, sufficiently far from the

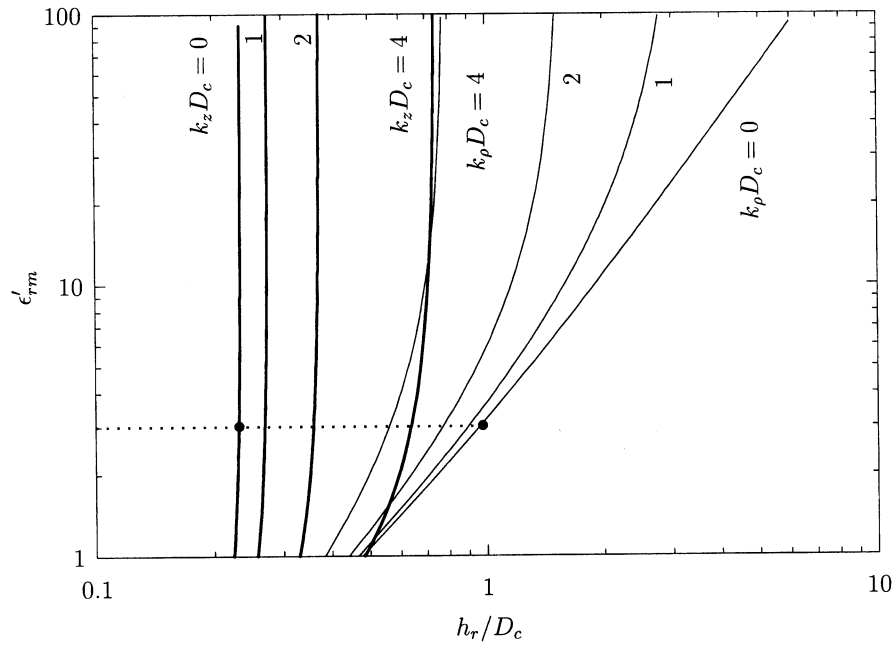

Fig. 4. Diagram depicting valid operating regions of the TE_{011} mode for fixture with a homogeneously filled circular guide.

resonator core, the field distribution is essentially due to a single waveguide mode. In the upper circular waveguide region, the field is essentially the TE_{01} circular waveguide mode with the z dependence, $e^{-k_z z}$. Similarly, in the radial waveguide region, the field is essentially the TE_{01} radial waveguide mode with the ρ dependence, $K_0(k_\rho \rho)$, where K_0 is the modified Bessel function. For resonance to occur the fields must decay in both waveguide regions. Therefore, the wavenumbers, k_z and k_ρ, must simultaneously be real and positive. A complex value of either k_z or k_ρ corresponds to a propagating wave in the circular or radial waveguide region, respectively.

Fig. 4 depicts the valid operating points of the TE_{011} mode for the dielectric rod configuration shown in Fig. 3(a). The operating boundaries are set by the cut-off conditions in the circular and radial waveguide regions, $k_zD_c = 0$ and $k_\rho D_c = 0$, respectively. The TE_{011} mode will not resonate for any point outside the $k_zD_c = 0$ and $k_\rho D_c = 0$ curves. Operating points outside these boundaries correspond to complex values of k_z or k_ρ, which are propagating waves in the circular or radial waveguides, respectively. For example, with $\epsilon'_{rm} = 3$, the TE_{011} mode will only resonate when h_r/D_c is between 0.16 and 0.97. For additional information concerning the behavior of the mode, curves at which k_zD_c and $k_\rho D_c = 1$, 2, and 4 are also included in Fig. 4. This provides useful information about the rates of decay in each of the waveguide regions for a particular operating point. In [5], a guideline, based on these rates of decay, for choosing the appropriate lengths (h_c and D_r) of waveguide regions is provided. To summarize, the lengths of the waveguide regions should be at least six times the decay length δ ($\delta = 1/k_{z,\rho}$) to avoid significant error in measuring the permittivity and loss tangent. If the primary concern is only in measuring the permittivity, the lengths need only be four times the decay length.

For the dielectric rod case, Fig. 5 is a graph of the normalized resonant frequencies, k_0D_c, as a function of h_r/D_c with ϵ'_{rm} as a parameter. In this graph, the left endpoints of these curves correspond to the cutoff condition in the circular guide, $k_zD_c = 0$, and the right endpoints correspond to the cutoff condition in the radial guide, $k_\rho D_c = 0$. Continuing the previous example, for $\epsilon'_{rm} = 3$ the normalized resonant frequency ranges from 3.15 to 4.39.

The same principles previously stated apply for the dielectric sheet case as well. Therefore, similar diagrams are presented with a brief explanation. Fig. 6 is a diagram depicting the valid operating points of the TE_{011} mode for the configuration shown in Fig. 3(c). Similar to the rod case, the operating boundaries are set by the cut-off conditions in the circular and radial waveguide regions, $k_zD_c = 0$ and $k_\rho D_c = 0$, respectively. For $\epsilon'_{rm} = 3$, the TE_{011} mode will only resonate when h_r/D_c is between 0.01 and 0.46. Curves at which k_zD_c and $k_\rho D_c = 1$, 2, and 4 are also included, again providing additional decay rate information.

For the dielectric sheet case, Fig. 7 is a graph of the normalized resonant frequencies as a function of h_r/D_c with ϵ'_{rm} as a parameter. In this graph, the left (or upper) endpoints of these curves correspond to $k_zD_c = 0$ and right endpoints are where $k_\rho D_c = 0$. For $\epsilon'_{rm} = 3$ the normalized resonant frequency ranges from 3.9 to 7.6.

The operating region and normalized frequencies for the configurations in Fig. 3(b) and (d) cannot be presented in simple figures because of the additional geometric parameters. The operating region and normalized frequencies can be presented for the configuration shown in Fig. 3(e), but they have not yet been made. Figs. 4–7 can be used, however, as rough guidelines for materials of other geometries.

IV. Measurement Procedure

The measurement procedure is composed of two steps, each requiring experimental measurements of the resonant frequency and quality factor. Using the Hewlett-Packard 8510C

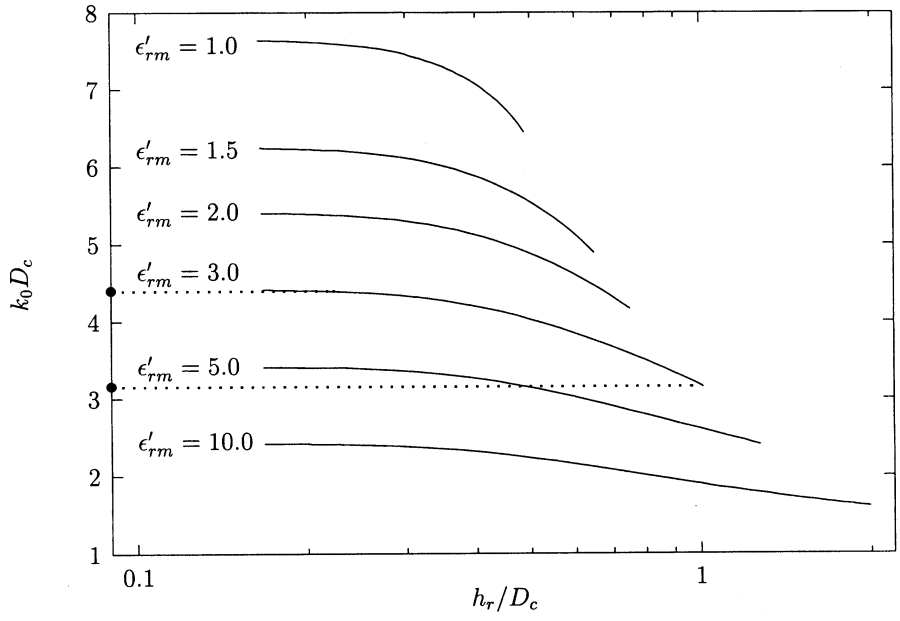

Fig. 5. Normalized resonant frequencies of the TE_{011} mode for fixture with a homogeneously filled circular guide.

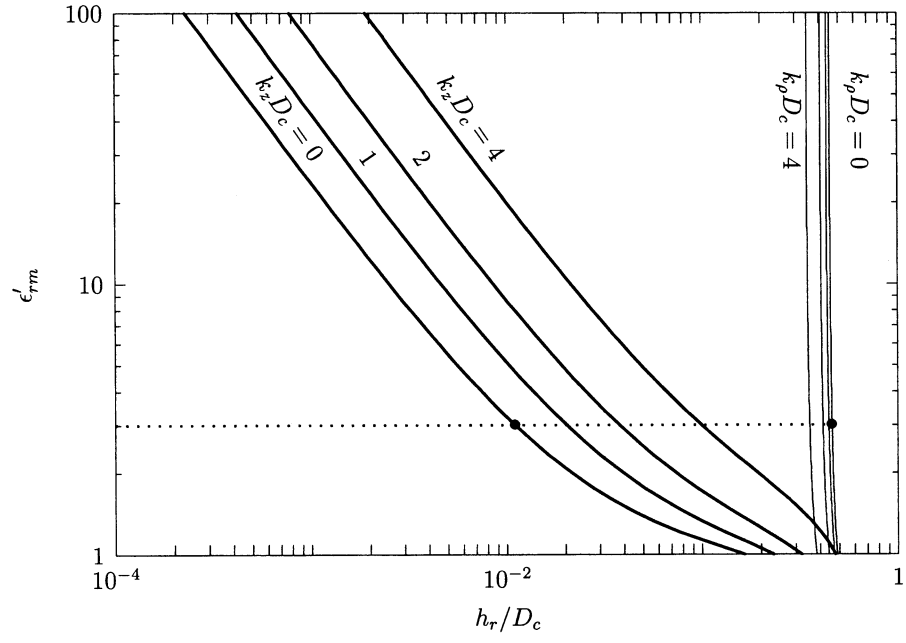

Fig. 6. Diagram depicting valid operating regions of the TE_{011} mode for fixture with a homogeneously filled radial guide.

network analyzer, the amplitude of the transmission coefficient, $|S_{21}|$, between the input probe and the output probe is measured. The peak of the $|S_{21}|$ response corresponds to the resonant frequency and the quality factor is related to the width of the $|S_{21}|$ response at the 3dB points.

In the first step, the surface resistance of the metal plates is determined. This is necessary to determine the conduction loss occurring on the surface of the metal walls in subsequent dielectric measurements. Notice in Figs. 4 and 6 that the curves extend down to $\epsilon'_{rm} = 1$. The described measurement fixture will resonate empty or air-filled, and the dielectric loss of air is insignificant. Therefore, for the air-filled resonator, the measured quality factor is essentially the quality factor due to the conduction loss, Q_c. Thus, using the electromagnetic field calculated by the FEM, the surface resistance can be calculated using known expressions. As a by-product of this portion of the measurement procedure, the permittivity of air can be determined from the measured resonant frequency. This is accomplished by varying the permittivity in a root-solving technique to match the measured resonant frequency to the FEM's calculated resonant frequency.

The second step of the measurement procedure determines the relative permittivity and loss tangent of the material under test. Again, with the measured resonant frequency, a root-solving technique is used with the FEM to determine the relative permittivity of the material under test. In doing

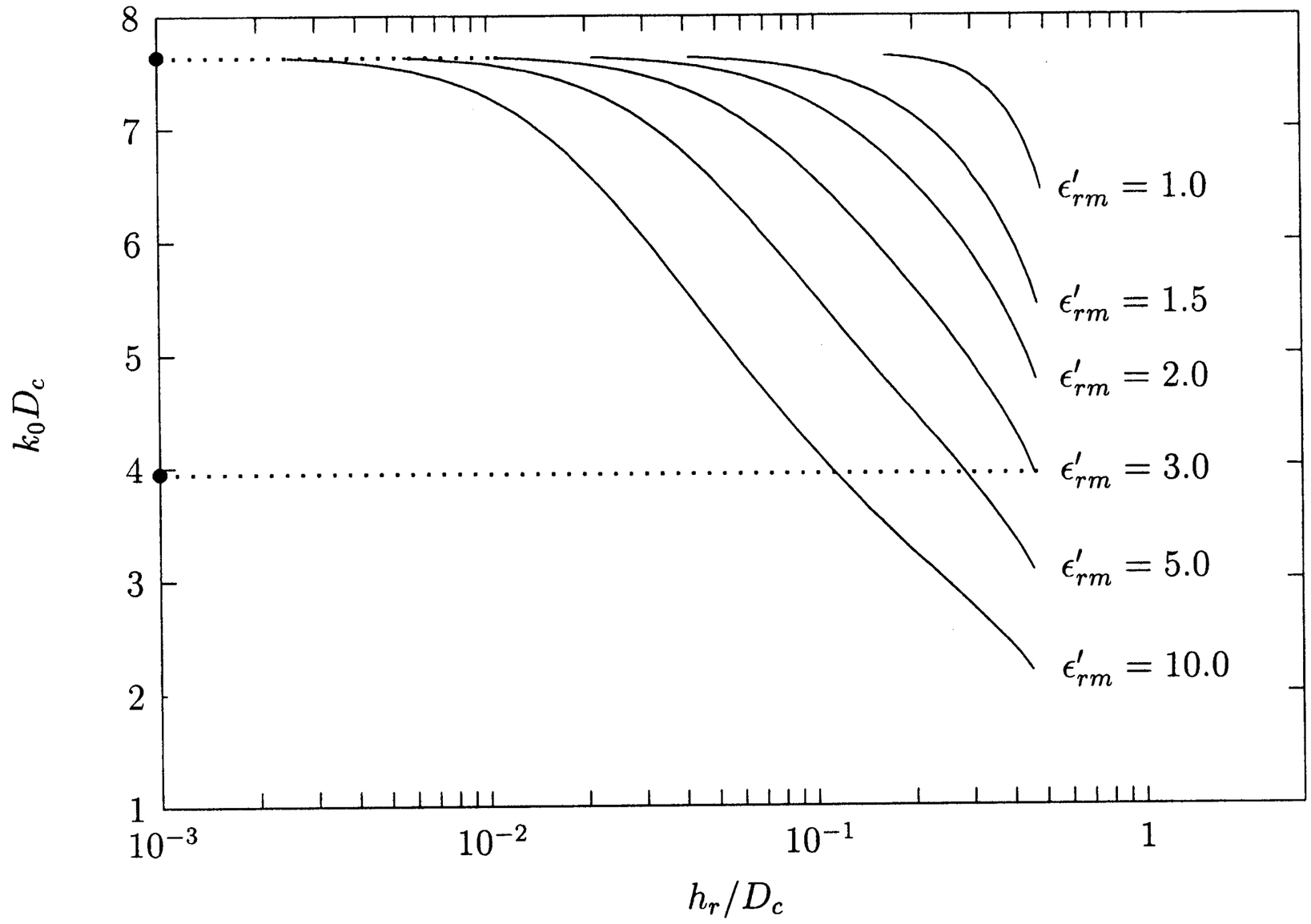

Fig. 7. Normalized resonant frequencies of the TE_{011} mode for fixture with a homogeneously filled radial guide.

so, the electromagnetic field is also calculated. With the measured quality factor, Q, and previously determined surface resistance, the calculated field is used to obtain Q_d, and thus, the loss tangent of the material can be determined.

In this work, typical finite-element meshes consisted of approximately 20 000 unknowns. This provided sufficient accuracy [5]. The FEM program was run on a 166 MHz Pentium with 64 Mb of RAM, and the run time of the program was less than 10 s.

V. Excitation and Detection of Resonance

In order to establish resonance, a probe is used to couple energy into the resonator. Ideally, the probe is designed to provide maximum coupling to the desired resonant mode and avoid coupling to other modes. A probe of the same design is used to detect the resonant behavior. The positioning of the probes is critical. Probes positioned too close to the core of the resonator will perturb the resonant behavior (field and frequency) causing incorrect results. If the probes are positioned too far from the core of the resonator, $|S_{21}|$ will be too small to measure. For the most accurate results, the probes are positioned such that the minimum measurable $|S_{21}|$ is obtained.

For the configurations shown in Fig. 3(a) and (b), the material under test occupies the circular waveguide region and the probes are positioned within the radial waveguide. For these measurements, simple loop-ended probes made from semi-rigid coaxial line are used. The coupling loops are oriented to maximize coupling to the H_z component of the resonant mode. In this case, a peak $|S_{21}|$ of -55 dB is easily obtained.

For the configurations shown in Fig. 3(c) and (d), the material under test occupies the radial waveguide region and the probes are positioned within the circular waveguide. In this case, when using loop-ended probes, the $|S_{21}|$ response was

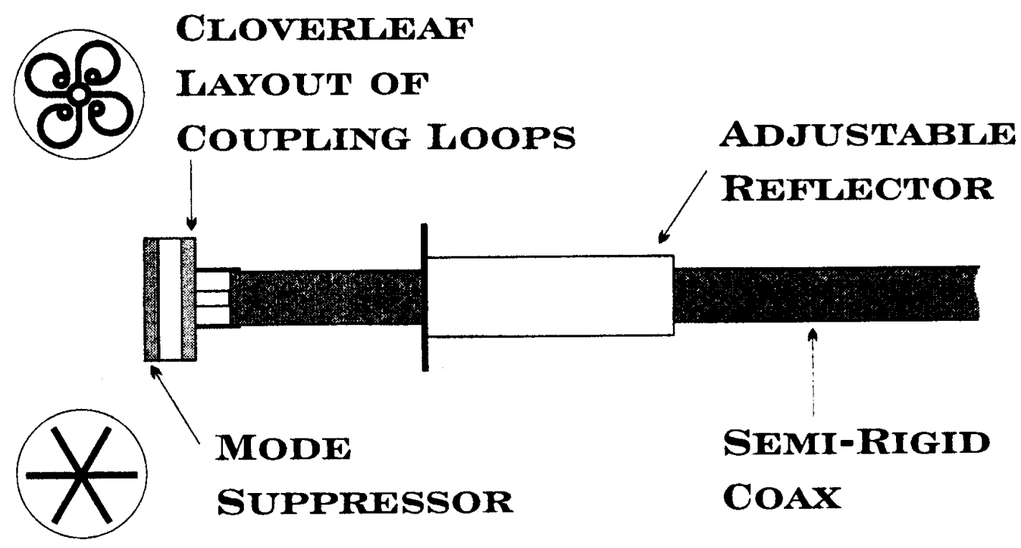

Fig. 8. Illustration of probe used to measure dielectric sheets and disks.

on average -22 dB with no discernible resonant peak. The loop-ended probes are unsatisfactory because of significant coupling to unwanted circular and coaxial[1] propagating modes, particularly at higher frequencies. Therefore, special probes were designed to perform the dielectric sheet measurements. Fig. 8 is an illustration of the design. A single probe consists of three major components; a radial mode suppressor, a *cloverleaf* layout of coupling loops, and an adjustable reflector. The radial mode suppressor is a series of radial metallic lines etched on pc board. Its function is to reduce the coupling to circular modes having a radially directed electric field component, E_ρ. The cloverleaf layout is a system of four coupling loops (also etched on pc board) all fed in phase. Its function is to reduce the coupling to circular modes with a ϕ-dependent H_z component. The adjustable reflector is made of a metallic disk attached to a section of tubing which is mounted on the body of the probe. This allows variable lengths between the coupling loops and the metallic disk. Its function is to minimize coupling to unwanted coaxial modes.

[1] With the probes positioned in the circular waveguide, the conducting walls of the fixture combined with the outer conductor of the probe form a coaxial waveguide.

TABLE I
MEASURED RESULTS FOR THE AIR-FILLED RESONATOR

h_r/D_c	f_0 (GHz)	Q	ϵ'_{ra}	$R_s/\sqrt{f_0}$ ($\times 10^{-7}$)
0.333	18.394	7830	1.0014	5.44
0.400	17.680	7000	1.0009	5.43

Depending on the frequency of interest, the radial mode suppressor and adjustable reflector can be used individually or in combination with the cloverleaf probe. At sufficiently low frequencies, the cloverleaf probe by itself provides very accurate results. For high frequency measurements, the use of these components yielded on average a peak $|S_{21}|$ response of -55 dB. Clearly, this represents an excellent design choice. A more detailed discussion concerning the design of the probe, its use, and quantified effects can be found in [5].

VI. EXPERIMENTAL RESULTS

The described measurement fixture was constructed to demonstrate the viability of this technique. The plates were machined from aluminum and the dimensions, as labeled in Fig. 1, are: $D_c = 19.08$ mm, $D_r = 152.42$ mm, $h_c - h_r = 105.92$ mm. The plate separation h_r is variable.

A. Characterizing the Surface Resistance

In Table I, the normalized surface resistance of the aluminum plates and the relative permittivity of air are presented for two values of h_r/D_c. The measured values of the permittivity of air compare well to the known value of air at atmospheric pressure, room temperature, and 50% humidity, $\epsilon'_{ra} = 1.000\,64$. The normalized surface resistance of aluminum, $R_s/\sqrt{f_0}$, when calculated using the DC values of conductivity, ranges approximately from 3.6×10^{-7} to 5.1×10^{-7}. However, using the DC value of conductivity to calculate $R_s/\sqrt{f_0}$ does not include the effects of surface roughness. Therefore, for subsequent dielectric measurements, the average of the measured values of $R_s/\sqrt{f_0}$ is used to calculate the conduction loss.

B. Dielectric Measurements

The measurement technique has been used to determine the dielectric properties of several types of materials. Results are presented, based on the geometry of the material in the following paragraphs. For each type of material, a table is presented which gives the normalized plate spacing, h_r/D_c, measured resonant frequency, measured quality factor, and finally, the determined permittivity and loss tangent of the material under test. For comparison purposes, Table II shows previously reported values, along with the source, of the various materials investigated in this work. The measured results presented in this work show excellent agreement with the previously reported values.

Using the configuration shown in Fig. 3(a), measurements were performed using Teflon, polystyrene, and acrylic (Lucite) rods. For each of the measurements, Table III shows the measured results for the dielectric rods. While the permittivities of the three rods are approximately the same, there is an order of magnitude higher loss for the acrylic rod. Also, note the consistency of the measurements for each material.

Using the configuration shown in Fig. 3(b), measurements were performed using a Teflon and acrylic (Lucite) tube: both of the tubes were air-filled. Table III shows the measured values for the dielectric tubes. Also using the configuration in Fig. 3(b), measurements were performed using the Teflon tube filled with mineral oil. Having previously determined the relative permittivity and loss tangent for the empty Teflon tube, any shift in resonant frequency and change in quality factor is due to the relative permittivity and loss tangent of the mineral oil, respectively. Thus, the electrical properties of the Teflon tube are held fixed in the finite-element model, and the relative permittivity and loss tangent of the mineral oil can be determined. This was done for two different values of h_r/D_c. Table III shows the measured results for the mineral

TABLE II
REPORTED VALUES OF MATERIALS INVESTIGATED IN THIS WORK

Material	ϵ'_{rm}	$\tan\delta_m$ ($\times 10^{-4}$)	Source
TEFLON	2.05-2.08	2.0-3.7	[8],[9]
POLYSTYRENE	2.5-2.55	3.3-4.9	[10]
ACRYLIC	2.5-3.0	32-50	[10],[9],[11]
STYCAST 1	7.5	-[a]	[12]
STYCAST 2	12.9	-	[12]
ALUMINA 1[b]	9.39-9.80	0.9-1.0	[13],[14]
ALUMINA 2[c]	9.35-10	0.20-0.27	[13],[15]
FUSED SILICA	3.83	20	[9],[16]
LSAT	22.8	1.0	[15]
$LaAlO_3$	23.7	0.20	[15]
MINERAL OIL	2.19	11-25	[17],[9]

[a]Not available
[b]Opaque alumina
[c]Transparent alumina

TABLE III
MEASURED RESULTS FOR VARIOUS DIELECTRIC RODS

Material	h_r/D_c	f_0 (GHz)	Q	ϵ'_{rm}	$\tan\delta_m$ ($\times 10^{-4}$)
TEFLON	0.333	12.964	2820	2.049	2.3
TEFLON	0.400	12.656	3130	2.044	2.1
TEFLON	0.500	12.054	3300	2.050	2.1
TEFLON	0.600	11.385	3450	2.047	2.2
TEFLON	0.666	10.926	3830	2.048	2.2
POLYSTYRENE	0.333	11.666	1720	2.539	4.4
POLYSTYRENE	0.400	11.406	1740	2.536	4.4
ACRYLIC	0.333	11.473	350	2.626	27
ACRYLIC	0.400	11.214	350	2.625	28
TEFLON TUBE	0.333	16.195	3870	2.032	3.0
ACRYLIC TUBE	0.333	16.988	850	2.624	33
MINERAL OIL	0.333	15.485	2670	2.196	16
MINERAL OIL	0.400	15.253	2820	2.207	16

TABLE IV
MEASURED RESULTS FOR THE VARIOUS DIELECTRIC SHEETS

Material	h_r/D_c	f_0 (GHz)	Q	ϵ'_{rm}	$\tan\delta_m$ ($\times 10^{-4}$)
TEFLON	0.083	18.239	4200	2.062	4.4
TEFLON	0.172	16.613	3760	2.059	3.0
TEFLON	0.251	15.252	3600	2.070	2.0
STYCAST 1	0.353	7.434	550	7.363	16
STYCAST 1	0.351	7.429	540	7.417	17
STYCAST 1	0.352	7.427	540	7.409	17
STYCAST 2	0.351	5.740	450	12.514	20
STYCAST 2	0.352	5.716	430	12.598	21
STYCAST 2	0.353	5.726	430	12.524	21
ALUMINA 1	0.040	14.143	6290	9.495	1.0
ALUMINA 1	0.081	11.266	5250	9.583	1.0
ALUMINA 1	0.121	9.830	4200	9.556	1.2
ALUMINA 2	0.015	17.501	9980	9.417	0.20
ALUMINA 2	0.017	17.173	10060	9.361	0.18
ALUMINA 2	0.032	15.054	9940	9.331	0.17
FUSED SILICA	0.073	16.230	3760	3.830	2.2
LSAT	0.027	11.633	4580	22.996	1.6
$LaAlO_3$	0.014	14.065	9110	23.725	0.37
$LaAlO_3$	0.027	11.421	9220	23.903	0.24
$LaAlO_3$	0.041	9.694	8540	23.812	0.22

TABLE V
MEASURED RESULTS FOR THE TEFLON DISKS

Material	D_m/D_c	h_r/D_c	f_0 (GHz)	Q	ϵ'_{rm}	$\tan\delta_m$ ($\times 10^{-4}$)
TEFLON	1.326	0.254	15.282	3560	2.044	1.9
TEFLON	1.661	0.254	15.265	3330	2.048	2.0
TEFLON	1.329	0.339	13.990	2810	2.049	2.2
TEFLON	1.654	0.339	13.930	2760	2.055	2.2
TEFLON	1.986	0.339	13.881	2750	2.068	2.2

oil. The ability to accurately measure the properties of tubes and liquids emphasizes the general utility of the technique.

Using the configuration shown in Fig. 3(c), measurements were performed using several dielectric sheets: Teflon, two types of Stycast and alumina, fused silica, LSAT, and Lanthanum Aluminate ($LaAlO_3$).

For each of the measurements, Table IV shows the measured values for the dielectric sheets. There is a 10 : 1 ratio in the permittivities of the materials measured, approximately a 20 : 1 ratio in the measured quality factors, and a 100 : 1 ratio in the loss tangent of the materials measured. It should be noted for the alumina #2 sample, that excellent results were obtained for the loss tangent even though the conduction loss was more than 10 times that of the dielectric loss ($Q_c = 10\,600$, $Q_d = 160\,500$).

Using the configuration shown in Fig. 3(d), measurements were performed using five different Teflon disks with diameter, D_m. The disks only partially fill the radial waveguide and a significant portion of the field will extend beyond the material. This is easily handled because of the full-wave analysis performed in the technique. Table V shows the measured values.

TABLE VI
MEASURED RESULTS FOR DIELECTRIC SPHERES

Material	h_r/D_c	f_0 (GHz)	Q	ϵ'_{rm}	$\tan\delta_m$ ($\times 10^{-4}$)
TEFLON	0.201	13.854	3040	2.066	2.2
TEFLON	0.879	8.836	3650	2.033	2.7

Using the configuration shown in Fig. 3(e), measurements were performed using two Teflon spheres. For each of the measurements, Table VI shows the measured values. The measured results for the spheres further illustrate the ability of the technique to handle more complex geometries.

VII. CONCLUSION

The authors have presented a measurement technique capable of measuring rotationally symmetric materials in general. The technique uses experimental measurements of the resonant frequency and quality factor along with a finite-element analysis of the fixture to determine the permittivity and loss tangent of the material under test. Experimental results compare very well with the previously reported values and demonstrate the flexibility of the measurement technique to handle a wide range of material geometries. This is possible because of the full wave analysis used in the measurement procedure.

REFERENCES

[1] W. R. Humbert and W. R. Scott, Jr., "A new technique for measuring the permittivity and loss tangent of cylindrical dielectric rods," *IEEE Microwave Guide Wave Lett.*, vol. 6, pp. 262–264, July 1996.
[2] ——, "Measurement of the permittivity and loss tangent of dielectric sheets," *Microwave Optical Tech. Lett.*, vol. 15, pp. 355–358, Aug. 20, 1997.
[3] G. Kent, "Dielectric resonances for measuring dielectric properties," *Microwave J.*, pp. 99–114, Oct. 1988.
[4] J. Jin, *The Finite Element Method in Electromagnetics*. New York: Wiley, 1993.
[5] W. R. Humbert, *A New Technique for Measuring the Electromagnetic Properties of Rotationally Symmetric Materials*, Ph.D. dissertation, Sch. Electric. Comput. Eng., Georgia Inst. Technol., Atlanta, 1997.
[6] E. L. Ginzton, *Microwave Measurements*. New York: McGraw-Hill, 1957.
[7] C. G. Montgomery, R. H. Dicke, and E. M. Purcell, Eds., *Principles of Microwave Circuits*. London, U.K.: Peregrinus, 1987.
[8] R. J. Cook, "Microwave cavity methods," in *High Frequency Dielectric Measurement*. Teddington, U.K.: IPC, Mar. 1972, pp. 12–27.
[9] A. von Hippel, Ed., *Dielectric Materials and Applications*. Boston, MA: Artech, 1954.
[10] B. W. Hakki and P. D. Coleman, "A dielectric resonator method of measuring inductive capacities in the millimeter range," *IEEE Trans. Microwave Theory Tech.*, vol. MTT-8, pp. 402–410, July 1960.
[11] D. R. Dreger, Ed., "Materials reference," *Machine Design Mag.*, vol. 56, pp. 95–189, Apr. 1984.
[12] Measured results provided by Georgia Technology Research Institute.
[13] Data obtained from manufacturer's specifications.
[14] R. K. Hoffman, Ed., *Handbook of Microwave Integrated Circuits*. Boston, MA: Artech, 1987.
[15] C. Zuccaro *et al.*, "Materials for HTS-shielded dielectric resonators," to be published, *IEEE Trans. Appl. Superconduct.*, June 1997.
[16] W. E. Courtney, "Analysis and evaluation of a method of measuring the complex permittivity and permeability of microwave insulators," *IEEE Trans. Microwave Theory Tech.*, vol. MTT-18, pp. 476–485, Aug. 1970.
[17] G. S. Smith, "On the skin effect approximation," *Amer. J. Phys.*, vol. 58, pp. 996–1002, Oct. 1990.

William R. Humbert was born in Newport News, VA, on April 6, 1965. He received the B.S. degree from Florida State University, Tallahassee, in 1990, and the M.S. and Ph.D. degrees from the Georgia Institute of Technology, Atlanta, in 1992 and 1997, respectively.

From 1992 to 1994, he worked as a Project Leader for the Real-Time Digital Beamforming Test Bed, Rome Laboratory, Air Force Research Laboratory, Hanscom AFB, MA. He is with the Electromagnetics Technology Division, Air Force Research Laboratory, Hanscom AFB. His research interests include computational electromagnetics, measurement of the electromagnetic properties of materials, and digitally beamformed phased array antennas.

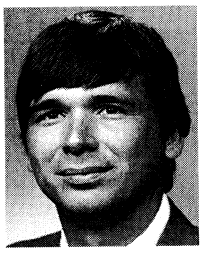

Waymond R. Scott, Jr. was born in Calhoun, GA, on April 6, 1958. He received the B.E.E., M.S.E.E., and Ph.D. degrees from the Georgia Institute of Technology, Atlanta, in 1980, 1982, and 1985, respectively.

From 1979 to 1980, he was a Student Assistant and Graduate Research Assistant at the Georgia Tech Research Institute, Atlanta, and from 1980 to 1985, he was a Graduate Research Assistant in the School of Electrical Engineering, Georgia Institute of Technology, where he is an Associate Professor of Electrical and Computer Engineering. His research interests include methods for detecting buried objects using both electromagnetic and acoustic waves, measurement of the electromagnetic properties of materials, transient electromagnetic fields, and numerical methods including the finite element and the finite-difference time-domain techniques.